Neural representations of statistical and rule-based predictions in Gilles de la Tourette syndrome

Adam Takacs, Eszter Toth-faber, Lina Schubert, Zsanett Tarnok, Foroogh Ghorbani, Madita Trelenberg, Dezso Nemeth, Alexander Münchau, Christian Beste

Received: 8 December 2023 | Revised: 11 April 2024 | Accepted: 6 May 2024

DOI: 10.1002/hbm.26719

RESEARCH ARTICLE

WILEY

Neural representations of statistical and rule-based predictions in Gilles de la Tourette syndrome

Adam Takacs[1,2] | Eszter Toth-Faber[3,4] | Lina Schubert[5] | Zsanett Tarnok[6] | Foroogh Ghorbani[1,2] | Madita Trelenberg[1] | Dezso Nemeth[7,8,9] | Alexander Münchau[5] | Christian Beste[1,2]

[1]Cognitive Neurophysiology, Department of Child and Adolescent Psychiatry, Faculty of Medicine, Technische Universität Dresden, Dresden, Germany

[2]University Neuropsychology Center, Faculty of Medicine, Technische Universität Dresden, Dresden, Germany

[3]Institute of Psychology, ELTE Eötvös Loránd University, Budapest, Hungary

[4]Brain, Memory and Language Research Group, Institute of Cognitive Neuroscience and Psychology, HUN-REN Research Centre for Natural Sciences, Budapest, Hungary

[5]Institute of Systems Motor Science, University of Lübeck, Lübeck, Germany

[6]Vadaskert Child and Adolescent Psychiatry Hospital and Outpatient Clinic, Budapest, Hungary

[7]INSERM, Université Claude Bernard Lyon 1, CNRS, Centre de Recherche en Neurosciences de Lyon CRNL U1028 UMR5292, Bron, France

[8]NAP Research Group, Institute of Psychology, Eötvös Loránd University and Institute of Cognitive Neuroscience and Psychology, HUN-REN Research Centre for Natural Sciences, Budapest, Hungary

[9]Department of Education and Psychology, Faculty of Social Sciences, University of Atlántico Medio, Las Palmas de Gran Canaria, Spain

Correspondence
Eszter Toth-Faber, Brain, Memory and Language Research Group, Institute of Cognitive Neuroscience and Psychology, HUN-REN Research Centre for Natural Sciences, Budapest, Hungary.
Email: toth-faber.eszter@ttk.hu

Funding information
Deutsche Forschungsgemeinschaft (DFG), Grant/Award Numbers: FOR 2698, TA1616/2-1; Agence Nationale de la Recherche, Grant/Award Number: N° ANR-22-CPJ1-0042-01; National Brain Research Program by Hungarian Academy of Sciences, Grant/Award Number: project NAP2022-I-1/2022

Abstract

Gilles de la Tourette syndrome (GTS) is a disorder characterised by motor and vocal tics, which may represent habitual actions as a result of enhanced learning of associations between stimuli and responses (S-R). In this study, we investigated how adults with GTS and healthy controls (HC) learn two types of regularities in a sequence: statistics (non-adjacent probabilities) and rules (predefined order). Participants completed a visuomotor sequence learning task while EEG was recorded. To understand the neurophysiological underpinnings of these regularities in GTS, multivariate pattern analyses on the temporally decomposed EEG signal as well as sLORETA source localisation method were conducted. We found that people with GTS showed superior statistical learning but comparable rule-based learning compared to HC participants. Adults with GTS had different neural representations for both statistics and rules than HC adults; specifically, adults with GTS maintained the regularity representations longer and had more overlap between them than HCs. Moreover, over different time scales, distinct fronto-parietal structures contribute to statistical learning in the GTS and HC groups. We propose that hyper-learning in GTS is a consequence of the altered sensitivity to encode complex statistics, which might lead to habitual actions.

Alexander Münchau and Christian Beste are shared senior authors.

KEYWORDS
electroencephalography, Gilles de la Tourette syndrome, multivariate pattern analysis, predictive processing, sequence learning, statistical learning, temporal decomposition

1 | INTRODUCTION

Gilles de la Tourette syndrome (GTS) is a disorder characterised by motor and vocal tics (M. M. Robertson et al., 2017). The nature of tics and GTS has been subject to debates about how to conceptualise them (Bartha et al., 2023; Beste & Münchau, 2018; Paulus et al., 2021) It has been proposed that tics represent habitual actions as a result of a higher tendency to form associations between stimuli and responses (S-R) (Beste & Münchau, 2018; C. Delorme et al., 2016; Kleimaker et al., 2020) and integrate them into sequential regularities through learning (Shephard et al., 2019; Takacs et al., 2021; Takács et al., 2018; Tóth-Fáber, Tárnok, Janacsek, et al., 2021). However, it is still unclear how this enhanced capability of learning affects memory representations in GTS and how this is mediated neurophysiologically. This, however, is a prerequisite to understand the emergence of habitual actions and how they might be modified in GTS. GTS participants typically show an enhanced sequence learning performance (Shephard et al., 2019; Takács et al., 2018; Tóth-Fáber, Tárnok, Janacsek, et al., 2021). It was suggested that this hyperlearning reflects an enhanced sensitivity to statistics (Takacs et al., 2021; Tóth-Fáber, Tárnok, Janacsek, et al., 2021), while the acquisition of rules might be impaired in GTS (Tóth-Fáber, Tárnok, Janacsek, et al., 2021). In the current study, we tested this assumption by directly comparing statistical and rule-based learning in GTS not only at a behavioural level but also as regards the stability of respective neural representations.

Cognitive functions, such as planning or grammar processing, rely on encoding and representing sequential information (Dehaene et al., 2015). Regularities within a sequence can be learnt by using different, partially overlapping learning processes (Conway, 2020; Maheu et al., 2019, 2022; Quentin et al., 2021; Takács et al., 2021)—such as statistical learning and rule-based learning. Statistical learning enables us to acquire probabilistic interrelations that can be used to make predictions above the chance level. Rules, on the other hand, allow deterministic forecasting in case of extreme statistical biases, that is, when uncertainty is low. It was shown that detecting the presence of regularity and assigning it to a learning process relies on two distinct yet simultaneously available sets of mental operations for statistics and rules (Maheu et al., 2022). This simultaneous nature of statistical and rule-based learning allows less costly computations than updating regularities in a single predictive system. For instance, representing multiple predictions concurrently enables the detection of sequential regularities on different timescales (Henin et al., 2021; Kóbor et al., 2018; Maheu et al., 2019). This idea was recently formalised from a neuronal network perspective in the dynamic predictive coding (DPC) model (Jiang & Rao, 2024) that presents a hierarchical framework for understanding how our neural networks predict spatiotemporal events. At the lower levels of this hierarchy, the model suggests that neural circuits form representations that capture sequences occurring over shorter timescales. These are the foundational elements of the model, where learning takes place through a bottom-up process, primarily relying on the encoding of perceptual features in a modular fashion. Conversely, at the higher levels, the model posits that neural circuits construct representations that comprehend sequences spanning longer or more intricate timescales, such as rules. This upper tier of the hierarchy influences the lower levels by employing prediction errors to modulate their temporal dynamics. Such interactions enable the model to generate temporal representations that are attuned to the inherent timescale of the sequential regularities being processed.

The DPC model aligns with the notion that while statistical learning is a predominantly bottom-up process, rule-based learning operates in a top-down manner, incorporating the statistical information that has been encoded automatically (Conway, 2020). When both statistical regularities and rule-based regularities are present in a sequence, it is plausible to expect the formation of two distinct neural representations, each dedicated to processing one type of regularity (Henin et al., 2021; Maheu et al., 2022), Building on the hierarchical interplay between these two forms of learning (Conway, 2020; Takács et al., 2021) it is suggested that the neural representations for statistical patterns are established prior to those for rules. This temporal precedence reflects the foundational role of statistical learning in the DPC model's architecture.

Additionally, statistical learning and rule-based learning could be differentiated based on the coding levels of the neurophysiological signal (Takács et al., 2021). Thus, sequential predictions based on either statistics or rules are likely supported by diverging neural correlates (Kóbor et al., 2018; Maheu et al., 2019; Simor et al., 2019; Takács et al., 2021). A previous study (Vékony et al., 2023) used temporal EEG signal decomposition and multivariate pattern analysis (MVPA) to investigate the contributions of perceptual, motor and abstract (i.e., not modality-specific) coding levels in the development of sequential memory representations. Neural representations of sequential regularities occurred at all three concomitant coding levels; however, statistics and rules were not analysed separately. Here, we followed the same protocol of MVPA on temporally decomposed EEG signal (Takács et al., 2022) to investigate how statistics and rule-based regularities are represented in GTS. Temporal decomposition analyses previously revealed that atypical S-R associations in GTS are related to the abstract (Kleimaker et al., 2020) rather than the modality-specific perceptual or motor coding levels (Beste & Münchau, 2018; Mielke et al., 2021).

Distinguishing between learning statistics and rules helped to elucidate the nature of cognitive alterations in a range of disorders (Farkas et al., 2021; Ullman & Pullman, 2015), including GTS (Tóth-Fáber, Tárnok, Janacsek, et al., 2021). It was suggested that

hyperlearning in GTS (Shephard et al., 2019;Takács et al., 2018; Tóth-Fáber, Tárnok, Janacsek, et al., 2021) reflects a dissociation between enhanced statistical learning (Takacs et al., 2021; Tóth-Fáber, Tárnok, Janacsek, et al., 2021) and impaired rule-based learning (Tóth-Fáber, Tárnok, Janacsek, et al., 2021). That is, lower-level temporal predictions (statistics) have an advantage over higher-level ones (rules) in GTS. We tested this assumption by directly comparing statistical and rule-based learning in GTS not only as behavioural performances but also as the stability of their respective neural representations. We expected that better learning would be reflected by either longer or a more accurately decodable representation in the neurophysiological signal. For a detailed explanation of how enhanced S-R associations, hyper-learning of statistics and the development of tics are mechanistically interrelated, we refer the reader to the review of Takacs et al. (2021).

We hypothesised that participants with GTS have a higher statistical learning score than healthy controls (HC) (Takács et al., 2018; Tóth-Fáber, Tárnok, Janacsek, et al., 2021). In contrast, we expected a lower rule-based learning score in the GTS than in the HC group (Tóth-Fáber, Tárnok, Janacsek, et al., 2021). We hypothesized that both statistical and rule-based information can be decoded from the neurophysiological signal (EEG) at all three (perceptual, motor and abstract) coding levels as in the study of Vékony et al., 2023. Additionally, we expected that statistical information at the abstract coding level can be observed either as a stronger (i.e., better decoding performance) or a longer maintained representation in GTS than in HC. To validate group differences in decoding performance, we compared their neural sources in a data-driven fashion (Takács et al., 2021; Vékony et al., 2023). We expected activation modulations of statistical learning in the precuneus, the angular gyrus, the inferior frontal and the superior frontal gyri (Park et al., 2022; Vékony et al., 2023); and of rule-based learning in the middle frontal and superior frontal gyri (Takács et al., 2021; Vékony et al., 2023).

2 | METHODS AND MATERIALS

2.1 | Participants

$N = 26$ adults with GTS and $N = 36$ neurotypical participants (HC) were recruited. One patient was excluded due to his consistently low accuracy (<70%) in the task. To match the 25 participants with GTS who were included (19 men, 6 women, $M_{age} = 34.12$ years, $SD_{age} = 10.31$ years, range between 20 and 55 years), we selected 25 HC participants on a one-to-one basis (14 men, 11 women, $M_{age} = 32.88$ years, $SD_{age} = 11.81$ years, range between 18 and 58 years). If a GTS participant had more than one valid match, we selected the one closest to him/her in age. All participants underwent a thorough clinical assessment that included a semistructured interview of tic severity (Yale Global Tic Severity Scale) (Leckman et al., 1989) and obsessive-compulsive symptoms (Yale Brown Obsessive Compulsive Scale, Goodman et al., 1989) and evaluation of lifetime tics (diagnostic confidence index, DCI, Robertson et al., 1999). Furthermore, a standardised video was taken of each participant (including HCs) and scored by two independent examiners using the modified rush videotape rating scale (Goetz et al., 1999). Total tic score could fall between 0 and 20, with a higher score indicating more frequent and more severe tics. When scores varied, all relevant parts of the standardised video were discussed until an agreement was reached. Participants also completed self-report questionnaires evaluating attentional deficit hyperactivity disorder (ADHD) symptoms (Conners' Adult ADHD Rating Scale, Christiansen et al., 2013) and OCD symptoms (obsessive-compulsive inventory-revised, Foa et al., 2002). Ten participants with GTS had comorbid diagnoses and 13 participants were taking medication. Patient characteristics can be found in Table 1. None of the participants in the matched HC group had any neurological, psychiatric or neurodevelopmental disorders or took centrally acting medication. All participants had normal or corrected-to-normal vision and hearing. IQ was measured with the Wechsler adult intelligence scale (Hartman, 2009). In both groups, the mean IQ was in the normal range and did not differ significantly between the two groups (GTS: 107.9 ± 10.11; HC: 110.0 ± 9.2; $t(48) = -0.754$, $p = 0.455$). In the HC group, 23 participants were right-handed and there were no left-handed participants, whereas in the GTS group, this ratio is 21 to 4. Data of two HC participants are missing. We compared these ratios with a Fisher's exact test and no significant effect emerged ($p = 0.111$).

HC participants were recruited from the Technical University of Dresden, the University of Lübeck and the Eötvös Loránd University; GTS participants were recruited from the University of Lübeck in Germany and the Hungarian Tourette Syndrome Society in Hungary. The assessment procedure, the EEG protocol and EEG equipment including the EEG caps and amplifiers were identical at the three measuring sites. Visits between the three sites were organised to monitor recruitment, experimental testing and data analyses. The assessment procedure and EEG protocol were identical at the three measuring sites. Written informed consent was obtained from all participants before they entered the study. The experiment was performed following the declaration of Helsinki and was approved by the ethics committees of the participating universities.

2.2 | Learning task, stimuli and analysis

Statistical and rule-based learning were tested with the cued version of the Alternating Serial Reaction Time (ASRT) task (Nemeth et al., 2013), which was adapted to EEG measurements (Kóbor et al., 2018). An arrow occurred at the centre of the screen as a target stimulus. Participants were instructed to press the corresponding button to the direction of the arrow as fast and as accurately as possible on a response pad (Figure 1a).

The presentation of the stimuli followed an 8-element sequence, where pattern and random elements alternated with each other (e.g., 1-r-2-r-3-r-4-r, where numbers indicate the four spatial directions [1 = left, 2 = up, 3 = down, 4 = right] and 'r' denotes a randomly selected direction out of the four possibilities). Pattern

TABLE 1 Clinical characteristics of the patients with GTS involved in the study.

Patient	Age	Sex	Disease duration (years)	DCI	YGTSS total (0–100)	YGTSS tics (0–50)	Rush score (0–20)	Y-BOCS score (0–40)	OCI-R score (0–72)	ADHD index (0–108)	Comorbidities	Medication
1	45	1	38	86	69	39	12	19	33	52	Depressive episode	Pimozide; Biperiden
2	21	1	3	83	16	16	8	10	16	4		
3	25	2	21	86	33	13	14	11	24	16		
4	47	1	32	66	15	15	13	0	0	4		
5	33	1	26	64	35	25	10	0	11	27		
6	25	2	21	54	6	6	5	0	6	6		
7	48	2	43	51	31	11	8	7	19	29	Depression, burnout	Escitalopram, Candesartan
8	28	2	23	55	31	21	16	18	14	24		
9	47	1	37	100	46	26	16	6	10	25	Depression	N/A
10	29	2	26	66	55	25	18	23	53	81	Borderline personality disorder, anxiety disorder, depressive episode	Alprazolam (if needed, every 2–3 weeks)
11	22	1	17	62	34	24	15	11	20	36		Aripiprazole
12	20	1	11	90	39	29	19	12	11	20		N/A
13	25	1	19	51	40	20	6	0	15	38	Depression	Pimozide
14	23	1	17	71	40	30	9	12	7	29	Depression, OCD, social phobia	Aripiprazole
15	54	1	48	65	51	21	15	17	15	50	Depression	Pantoprazol, Paroxetine, Simvastatin, Korodin (if needed), Mirtazapine (if needed), Mometasonfuroat, Sumatriptan
16	50	1	ca. 40	38	0	0	3	0	0	3		Aripiprazole
17	40	1	34	85	26	16	14	12	26	35	OCD	Citalopram
18	21	2	14	93	37	17	15	14	33	40		
19	37	1	32	100	57	37	14	3	5	40	ADHD, depressive episode	N/A
20	35	1	29	53	41	21	16	0	2	25	ADHD	Methylphenidate
21	30	1	24	48	18	18	N/A	0	15	N/A		
22	35	1	26	49	27	47	N/A	14	44	N/A		
23	35	1	25	45	20	20	N/A	2	10	N/A		
24	33	1	23	88	18	38	N/A	0	20	N/A		
25	42	1	17	76	25	45	N/A	2	7	N/A		
Mean	34		25.25	69	32.40	23.20	12.30	7.72	16.64	29.20		

Note: The Rush score is missing for five patients due to a technical error. The ADHD index is missing for five patients due to the unavailability of the Conners' adult rating scale in the hospital site in Hungary.

Abbreviations: ADHD index, Conners' ADHD adult rating scale; DCI, diagnostic confidence index; GTS, Gilles de la Tourette syndrome; OCI-R, obsessive-compulsive inventory-revised; Rush, rush video-based tic rating-scale; Y-BOCS, Yale brown obsessive compulsive scale; YGTSS, Yale global tic severity scale.

elements were shown in black, while random elements were red. Participants were instructed to find the pattern of the black arrows' directions. They did not receive information about the exact sequence structure.

In the task, three successive trials are referred to as triplets and the alternating sequence makes some triplets more probable than others. Given the example sequence, 1-r-2-r-3-r-4-r, 1-X-2, 2-X-3, 3-X-4 and 4-X-1 (where X refers to the middle element of the triplet) appeared with a higher probability as their third trials could be either pattern or random. To the contrary, 1-X-3 and 2-X-4 appeared with a lower probability as their third elements could only be random. Furthermore, high-probability triplets could be further distinguished based on their structure: they could be either pattern-ending or random-ending triplets. It is important to note that performance is not quantified on the triplet-level; instead, performance (i.e., accuracy or reaction time) is always calculated only on the last trial of a triplet. Each trial was categorised as the third trial of either a high-probability or a low-probability triplet and also either as pattern or random elements (note that they are also visually distinguishable).

In the task, there are 64 unique triplets (including all pattern–random–pattern [50%] and random–pattern–random [50%] triplets), of which 16 are high-probability and 48 are low-probability triplets. Concerning high-probability triplets, four possible combinations are present in regard to the first and third trials of the triplet (1-X-2, 2-X-3, 3-X-4, 4-X-1 for the example sequence) with four possible arrow directions for the middle trial. High-probability triplets account for 62.5% of all trials as they can occur as pattern–random–pattern (50%) and by 1/4 chance as random–pattern–random triplets (12.5%) (Figure 1c). In the case of low-probability triplets, the first and the second trials of the triplet may point in either of the four directions, whereas the last trial has three possible directions as the fourth direction corresponds to a high-probability triplet. Thus, low-probability triplets constitute 37.5% of all trials. As noted above, all low-probability triplets have a random–pattern–random structure. On the level of unique triplets, high-probability triplets are five times more probable than the low-probability ones (4% [62.5%/16] vs. 0.8% [37.5%/48]).

Given the probability and the structure, we can distinguish between three trial types: (1) trials that are the last elements of a high-probability triplet and are part of the predetermined sequence called high-probability pattern trials, (2) random trials that are the final elements of a high-probability triplet termed high-probability random trials and (3) random trials that are the final elements of a low-probability triplet called low-probability random trials (Figure 1c).

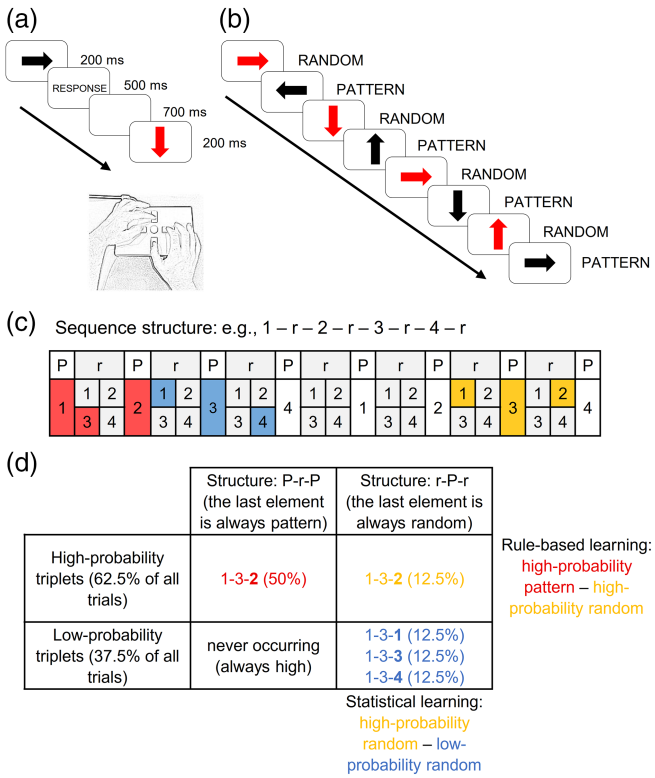

FIGURE 1 The alternating serial reaction time task. (a) In the task, arrows occurred in the middle of the screen and participants were asked to press the corresponding key on the response pad using the thumb and index finger of both hands. The stimulus was displayed at the centre of the screen for 200 ms. Next, a blank screen was presented until a response was given but no longer than 500 ms. Then, a 700-ms-long fixed delay with a blank screen was followed by the next trial. In case of an incorrect response, a blank screen was displayed followed by an 'X', presented for 500 ms in the middle of the screen. In case of no response within the 500-ms-long response window, a '!' was presented for 500 ms. (b) The presentation of stimuli followed an 8-element sequence where pattern and random trials alternated with each other. (c) Due to the alternating sequence, some triplets are presented with a higher probability than others. Given the example sequence, 1-r-2-r-3-r-4-r (where numbers denote the four spatial directions [1 = left, 2 = up, 3 = down, 4 = right] and 'r' indicates a randomly selected direction out of the four possibilities), 1-X-2, 2-X-3, 3-X-4 and 4-X-1 (where X refers to the middle element of the triplet) appeared with a higher probability as their third trials could be either pattern or random. To the contrary, 1-X-3 and 2-X-4 appeared with a lower probability as their third elements could only be random. (d) Moreover, high-probability triplets could be further distinguished based on their structure: they could be either pattern-ending or random-ending triplets. Based on probability and structure, three trial types can be differentiated: (1) trials that are the last elements of a high-probability triplet and are part of the predetermined sequence called high-probability pattern trials (marked with red shading and font), (2) random trials that are the final elements of a high-probability triplet termed high-probability random trials (marked with yellow shading and font) and (3) random trials that are the final elements of a low-probability triplet (marked with blue shading and font). Please note that the percentages refer to the frequency of occurrence of the unique triplet (for details, see the main text). To calculate statistical learning, accuracy performance on low-probability random trials is extracted from performance on high-probability random trials. To quantify rule-based learning, accuracy performance on high-probability random trials is extracted from performance on high-probability pattern trials. For RT performance, the extractions are reversed. This way, regarding both accuracy and RT, a higher learning score indicates better learning. The first five random practice trials and the first two elements of the first triplet were also excluded from the analyses. Figure was adapted from Nemeth et al. (2013).

We calculated how accurate and how fast people were in the three trial categories. The remaining trials were categorised into conditions in a moving window way along the stimulus stream. A given trial was included as the third trial of a triplet (as a predicted item); the same trial was then also included as the middle (interim item), and lastly as the first trial (as a predictor item) of the next two triplets. The stimuli were shown in 40 blocks, each with 85 trials. For the behavioural analysis, we analysed time windows in 5-block units (Howard et al., 2004; Nemeth et al., 2013). For each person and each 5-block unit, we calculated the average accuracy and the median RT separately for high-probability random, low-probability random and high-probability pattern trials. Statistical learning was defined as the difference between responses to high-probability random and low-probability random trials. Rule-based learning was defined as the difference between responses to high-probability pattern and high-probability random trials. For both learning scores, a bigger difference between trial types indicates better learning (Figure 1c).

It is important to note that the distinction of statistical and rule-based learning is not unique to the cued ASRT task. Previous studies showed that after excessive (4-day-long or 9-day-long) training, rule-based learning appears even in the uncued ASRT task (Éltető et al., 2022; Howard et al., 2004; Howard Jr. & Howard, 1997), which shares an identical underlying structure with the cued ASRT task but does not visually distinguish pattern and random trials. The visual distinction of pattern and random trials enables that statistical and rule-based learning can be measured within the same time frame, that is, in one learning session.

During the task and EEG recording, GTS participants were not instructed to suppress tics. The task was presented in 2-minute-long blocks with short self-paced breaks between them, which could have helped managing tics during the task. To examine whether possible tic events influenced performance on the behavioural task, we checked baseline performance (i.e., baseline accuracy and reaction times on the task, which are independent of the regularities in the task) and the number of missed responses. No difference was found between the GTS and HC groups.

Please note, that statistical learning scores have been reported elsewhere (Takacs et al., 2024), as part of a separate analysis on how the resting-state network architecture is related to learning non-adjacent probabilities.

2.3 | EEG recording and segmentation

EEG was recorded with 60 Ag/AgCl electrodes (EasyCap, Germany) and a BrainAmp amplifier (Brain Products GmbH, Gilching, Germany), controlled by Brain Vision Recorder 1.2. The electrode layout was based on the standard 10%-system with equidistant scalp positions. The coordinates of $\theta = 58$, $\varphi = 78$ and $\theta = 90$, $\varphi = 90$ were used for ground and reference, respectively. Impedances were kept below 10 kΩ. EEG was recorded at a sampling rate of 500 Hz. The data were preprocessed by using Automagic (Pedroni et al., 2019) and EEGLAB (A. Delorme & Makeig, 2004) on Matlab 2019a (The MathWorks Corp., Massachusetts, USA). First, flat channels were removed, and the recordings were re-referenced to an average reference. Second, the PREP preprocessing pipeline (Bigdely-Shamlo et al., 2015) was applied. PREP removes line noise at 50 Hz using a multitaper algorithm and applies a robust average reference after removing contaminations by bad channels. Flat-line, noisy and outlier channels were detected and removed. A high-pass filter of 0.5 Hz and a low-pass filter of 40 Hz were used (sinc FIR filter, order: 86) (Widmann et al., 2015). EOG artefacts were removed by following a subtraction method (Parra et al., 2005). Muscular and remaining eye artefacts were automatically classified and removed by using an independent component analysis based multiple artifact rejection algorithm (Winkler et al., 2014, 2011). Components containing cardiac artefacts were identified and removed by using ICLabel (Pion-Tonachini et al., 2019). Finally, all removed channels were interpolated in a spherical fashion.

The pre-processed data were segmented in Brain Vision Analyzer (Brain Products GmbH), separately for high-probability pattern, high-probability random and low-probability random conditions. Segments started −200 ms and ended 750 ms relative to stimulus onset. Only segments with correct responses were included. We applied current-source density (CSD) transformation with four orders of splines (Kayser & Tenke, 2015; Perrin et al., 1989) as a reference-free spatial filter. Next, the segmented data were baseline-corrected based on the 200 ms interval before the stimulus onset. Finally, the data were exported to Matlab for temporal signal decomposition (residue iteration decomposition; RIDE). Separate datasets were also created without CSD transformation specifically for the source localisation analyses.

2.4 | Neurophysiological analyses

2.4.1 | Residue iteration decomposition

We used RIDE (Ouyang et al., 2011; Ouyang & Zhou, 2020) in Matlab 2019a (The MathWorks Corp.) as part of the RIDE-MVPA protocol (Takács et al., 2022) to perform temporal signal decomposition. RIDE uses estimated clusters with different latency information (variable vs. static), which are then self-optimised by applying a nested iteration scheme. The procedure is based on segmented single-trial EEG data and performed on each channel separately. RIDE was applied to estimate three clusters: S-cluster ('stimulus cluster') captures information on stimulus-related processes, such as perception and attention; C-cluster ('central cluster') covers intermediate or translational processes between stimulus and response, such as decision-making or response selection; R-cluster ('response cluster') refers to motor preparation and execution (Ouyang & Zhou, 2020). We have selected time windows of initial cluster estimation based on previous studies that used RIDE in EEG data with the ASRT paradigm (Takács et al., 2021; Vékony et al., 2023): 150–600 ms after stimulus presentation for the C-cluster, 0–500 ms after stimulus onset for the S-cluster and the time window between 300 ms before and 300 ms after the

response markers for the R-cluster. To estimate a given cluster, RIDE subtracts the other two clusters from the single-trial EEG and aligns the residuals from every trial to the latency of the estimated cluster. As a result, the estimated cluster represents the median waveform. Previous studies have shown that the final cluster solution represents a conceptually meaningful separation of simultaneous coding levels in the EEG signal (Opitz et al., 2020; Ouyang & Zhou, 2020; Wolff et al., 2017). Finally, single-trial data at the subject level was exported for multivariate analyses.

2.4.2 | Multivariate pattern analysis (MVPA)

MVPA were performed by using the MVPA-light toolbox (Treder, 2020) in Matlab 2019a (The MathWorks Corp.). See the RIDE-MVPA protocol (Takács et al., 2022) for further details. Classes of high-probability random and low-probability random were decoded separately for the three RIDE-decomposed clusters to identify the neurophysiological representation of stimulus probability. We refer to this as the decoding of 'statistical information'. Classes of high-probability random and high-probability pattern were decoded separately for the three RIDE-decomposed clusters to identify the neurophysiological representation of the alternating sequence order. We refer to this as the decoding of 'rule-based information'. For both types of class differences, temporal generalisation was calculated to analyse the temporal dynamics and the representational stability of statistical learning and rule-based learning, respectively. To avoid overfitting, we used under-sampling to even trial numbers between classes (Treder, 2020). All 60 EEG channels were used as classification features. Decoding and temporal generalisation were computed for each individual and each RIDE-cluster. We used an L1-Support Vector Machine (SVM) as a classifier to decode statistical information and rule-based information. SVM outperforms the default linear discriminant analysis when the data are non-Gaussian, noisy or prone to outliers (Treder, 2020). We applied five-fold cross-validation to the classifications. The procedure splits the data into five equal parts. In each iteration step, one part was dedicated to testing and the rest for training. After each fold had been used for testing, the average of the iterations was saved as a final result. To find the time interval where the classes differed, we used the area under the curve (AUC) as a measure of decoding performance and compared it to the chance level of AUC = 0.5 with Wilcoxon-tests for each time point across participants. We used cluster-based permutation (1000 permutations) as a method of statistical correction.

When the brain represents a set of similar stimuli as a unified percept based on their summary statistics (i.e., mean, range, variance, etc.), those are often referred to as set or 'ensemble representations' (Ariely, 2001; Bayne & McClelland, 2019; Corbett et al., 2023). Ensembles compress real-life experiences by collapsing similar and redundant information while integrating them into preexisting internal models of environmental statistics (Hansmann-Roth et al., 2021; Khayat et al., 2023). Ensemble representations develop in an automatic, implicit fashion not only for perceptual or low-level features (i.e., distance, location) but also for high-level ones, such as semantic categories (Chang & Gauthier, 2022; Khayat et al., 2021, 2023). We used multivariate decoding methods to analyse representation dynamics of sequential predictability information irrespective of their physical properties (see also Vékony et al., 2023). The classes we used for decoding differed only in their (high-level) properties of either statistical or rule-based predictability, while low-level features, such as the colour or orientation of the presented stimuli were balanced between classes. Thus, we interpret the decoded patterns as neural ensemble representations of statistical information and rule-based information.

2.4.3 | Source localisation analysis (sLORETA)

Source localisation was performed in the standardised low-resolution brain electromagnetic tomography (sLORETA) software package (Pascual-Marqui et al., 2002). The procedure has been shown to provide reliable source estimations coinciding the TMS and high-resolution MR scanning (Dippel & Beste, 2015). sLORETA was used by employing a three-shell spherical head model (MNI152 template), in which the intracerebral volume is partitioned into 6239 voxels with a 5 mm spatial resolution. The standardised current density is calculated for every voxel of the model. sLORETA provides a single linear solution for the inverse problem without localisation bias (Marco-Pallarés et al., 2005; Pascual-Marqui et al., 2002; Sekihara et al., 2005). Voxel-wise randomisation with 5000 permutations in the statistical non-parametric mapping procedures (SnPM) was used to correct for multiple comparisons. The sLORETA was performed in a data-driven fashion to support the behavioural and MVPA results. Therefore, only C-cluster data were analysed. We compared high-probability random and low-probability random conditions to analyse activation differences related to statistical learning; and high-probability random and high-probability pattern conditions for estimating sources of rule-based learning. The comparisons were conducted separately in the GTS and HC groups. As the behavioural results showed a group difference in statistical learning, differential activity was calculated for the high-probability random and low-probability random contrast between GTS and HC. To identify functional neuroanatomical regions showing learning effects, interval that were decoded significantly above-chance were averaged for the sLORETA (Petruo et al., 2021; Prochnow et al., 2021; Vékony et al., 2023). Additionally, time windows with high temporal generalisation (see 'Neurophysiological results') were selected and averaged for source localisation. sLORETA results are described in Table 2 and depicted in Figure 3.

TABLE 2 Source localisation results.

	HC		GTS		
	Statistical learning	**Rule-based learning**	**Statistical learning**	**Rule-based learning**	**Statistical learning difference**
Decoding interval	I. Sub-gyral BA39, MNI: −30, −60, 30 II. Angular gyrus BA39, MNI: −40, −80, 30 III. Precuneus BA19, MNI: −40, −80, 35	I. Precentral gyrus BA9, MNI: −35, 5, 40 II. Sub-lobar BA6, MNI: 40, −15, 15 III. Precuneus BA31, MNI: −15, −60, 25	I. Entorhinal cortex BA28 MNI: 20, 5, −35 II. Perirhinal cortex BA36 MNI: 20, 0, −35	I. Lingual gyrus BA18 MNI: 10, −100, −10 II. Cuneus BA17 MNI: 10, −100, −5	I. Precentral gyrus BA4, MNI: 65, −10, 30 II. BA6, MNI: 65, 5, 25
Generalisation interval	I. Sub-gyral BA39, MNI: −30, −60, 30 II. Angular gyrus BA39, MNI: −40, −80, 30 III. Precuneus BA19, MNI: −40, −80, 35	I. Sub-lobar BA13, MNI: 40, −15, 15 II. Inferior frontal gyrus BA9, MNI: −35, 5, 30	I. Medial frontal gyrus BA9, MNI: −20, 35, 20 II. Superior frontal gyrus BA10, MNI: −25, 45, 25	I. Inferior parietal lobule BA40, MNI: −55, −60, 40 II. Angular gyrus BA39, MNI: −55, −60, 35	I. Inferior frontal gyrus BA44, MNI: −60, 5, 15 II. Precentral gyrus BA44, MNI: −60, 10, 15

Note: Decoding interval refers to time windows that were decoded significantly above chance level. Generalisation interval refers to tie windows with high temporal generalisation (see Neurophysiological results for specific time windows). The first four columns present activity changes related to specific learning processes (i.e., differences between experimental conditions) separately in the GTS and HC groups. The last column presents differential activity between the two groups in statistical learning. Results are specified as Broadmann areas (BA); and Montreal Neurologic Institute (MNI) coordinates as [x,y, z]. See also Figure 3.

Abbreviations: GTS, Gilles de la Tourette syndrome; HC, healthy controls.

3 | RESULTS

3.1 | Behavioural results

Statistical learning was tested with a mixed-design ANOVA on accuracy scores with Group (GTS vs. HC) as a between-subject factor and Probability (high-probability random vs. low-probability random trials) and Block (blocks 1–5, blocks 6–10, blocks 11–15 and blocks 16–20) as within-subject factors. In baseline accuracy scores (i.e., accuracy scores irrespective of trial types), the ANOVA showed no differences between the GTS and HC groups (non-significant main effect of Group, $F(1, 48) = 1.47$, $p = 0.231$, $\eta^2_p = 0.030$). Baseline accuracy scores did not change over the task (non-significant main effect of Block, $F(3, 144) = 0.623$, $p = 0.601$, $\eta^2_p = 0.013$; non-significant Block × Group interaction: $F(3, 144) = 0.31$, $p = 0.815$, $\eta^2_p = 0.006$). Overall, significant statistical learning occurred on the task (significant main effect of Probability, $F(1, 48) = 17.56$, $p < 0.001$, $\eta^2_p = 0.268$). Participants showed higher accuracy on high-probability random trials ($M = 93.27\%$) compared with low-probability random trials ($M = 91.93\%$). Moreover, statistical learning changed as the task progressed: participants did not differentiate between high-probability random and low-probability random trials in blocks 1–5 ($M_{\text{high-probability random}} = 92.38\%$, $M_{\text{low-probability random}} = 92.37\%$, $p = 0.996$), learning became significant in blocks 6–10 ($M_{\text{high-probability random}} = 94.37\%$, $M_{\text{low-probability random}} = 91.65\%$, $p < 0.001$), did not reach significance in blocks 11–15 ($M_{\text{high-probability random}} = 93.02\%$, $M_{\text{low-probability random}} = 91.99\%$, $p = 0.173$) and was significant in blocks 16–20 ($M_{\text{high-probability random}} = 93.30\%$, $M_{\text{low-probability random}} = 91.69\%$, $p = 0.004$). Crucially, we found differences between the GTS and HC groups in the magnitude of learning (as indicated by the significant Probability × Group interaction: $F(1, 48) = 4.032$, $p = 0.05$, $\eta^2_p = 0.077$). The follow-up ANOVA on the learning scores showed higher statistical learning in the GTS group ($M = 1.99\%$) compared with the HC group ($M = 0.699\%$) (Figure 2). The trajectory of statistical learning was comparable between the groups (non-significant Probability × Block × Group interaction, $F(3, 144) = 1.35$ $p = 0.262$, $\eta^2_p = 0.027$).

An identical mixed-design ANOVA was run on RTs as well. In baseline RTs (i.e., RTs irrespective of trial types), the ANOVA revealed no differences between the GTS and HC groups (non-significant main effect of Group, $F(1, 48) = 2.518$, $p = 0.119$, $\eta^2_p = 0.050$). Baseline RTs decreased as the task progressed (significant main effect of Block, $F(3, 144) = 30.809$, $p < 0.001$, $\eta^2_p = 0.391$), participants became faster with practice concerning all trials, but this decrease in RTs did not differ between the groups (non-significant Block × Group interaction: $F(3, 144) = 0.972$, $p = 0.408$, $\eta^2_p = 0.020$). Overall, participants showed significant statistical learning on the task (significant main effect of Probability, $F(1, 48) = 149.934$, $p < 0.001$, $\eta^2_p = 0.757$) and the magnitude of learning changed over the task (significant Probability × Block interaction, $F(3, 144) = 13.665$, $p < 0.001$, $\eta^2_p = 0.222$). The overall learning (non-significant Probability × Group interaction, $F(1, 48) = 0.718$, $p = 0.401$,

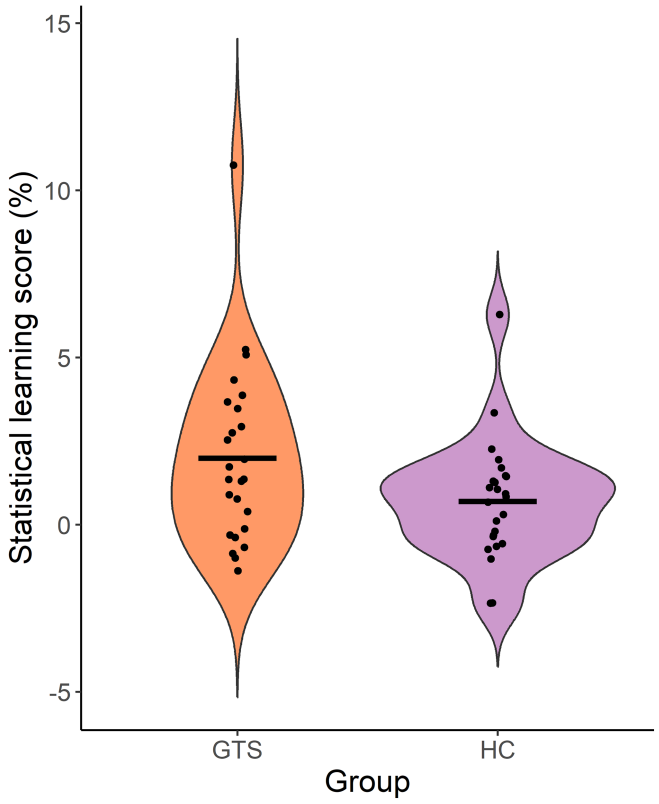

FIGURE 2 Statistical learning performance. Statistical learning scores averaged over the whole task length are shown separately in the GTS (left/orange) and HC (right/purple) groups. The plot represents probability density of the statistical learning score. Individual data points are depicted as black dots and the groups' mean are represented by the black line.

$\eta^2_p = 0.015$) and the trajectory of learning (non-significant Probability × Block × Group interaction: $F(3, 144) = 1.400$, $p = 0.245$, $\eta^2_p = 0.028$) were comparable between the groups.

Rule-based learning was tested with a mixed-design ANOVA on accuracy scores with Group (GTS vs. HC) as a between-subject factor and Order (high-probability pattern vs. high-probability random trials) and Block (blocks 1–5, blocks 6–10, blocks 11–15 and blocks 16–20) as within-subject factors. The GTS and HC groups showed similar baseline accuracy scores (non-significant main effect of Group, $F(1, 48) = 1.222$, $p = 0.275$, $\eta^2_p = 0.025$) and baseline accuracy scores did not change throughout the task (non-significant main effect of Block, $F(3, 144) = 1.336$, $p = 0.265$, $\eta^2_p = 0.027$; non-significant Block × Group interaction: $F(3, 144) = 1.461$, $p = 0.228$, $\eta^2_p = 0.030$). The ANOVA confirmed significant rule-based learning (main effect of Order, $F(1, 48) = 13.44$, $p < 0.001$, $\eta^2_p = 0.219$), participants showed higher accuracy scores on high-probability pattern ($M = 94.86\%$) compared to high-probability random trials ($M = 93.27\%$). The accuracy difference between high-probability pattern and high-probability random trials changed as the task progressed (Order × Block interaction, $F(3, 144) = 2.693$, $p = 0.048$, $\eta^2_p = 0.053$), with significant learning in blocks 1–5 ($M_{\text{high-probability pattern}} = 94.82\%$, $M_{\text{high-probability random}} = 92.38\%$, $p < 0.001$), blocks 11–15 ($M_{\text{high-probability pattern}} = 95.06\%$, $M_{\text{high-probability random}} = 93.02\%$, $p = 0.005$) and blocks 16–20 ($M_{\text{high-probability pattern}} = 95.08\%$, $M_{\text{high-probability random}} = 93.30\%$, $p = 0.026$), but not in blocks 6–10 ($M_{\text{high-probability pattern}} = 94.48\%$, $M_{\text{high-probability random}} = 94.37\%$, $p = 0.887$). We did not find any differences in overall rule-based learning (non-significant Order × Group interaction, $F(1, 48) = 0.438$, $p = 0.511$, $\eta^2_p = 0.009$) or in the trajectory of learning (non-significant Order × Block × Group interaction, $F(3, 144) = 0.196$, $p = 0.899$, $\eta^2_p = 0.004$) between the groups.

An identical mixed-design ANOVA was also conducted on RTs. Baseline RTs were comparable between the groups (non-significant main effect of Group, $F(1, 48) = 0.655$, $p = 0.422$, $\eta^2_p = 0.013$). RTs gradually decreased as the task progressed, irrespective of trial types (significant main effect of Block, $F(3, 144) = 37.379$, $p < 0.001$, $\eta^2_p = 0.438$) and this decrease was similar in the groups (non-significant Block × Group interaction: $F(3, 144) = 0.936$, $p = 0.396$, $\eta^2_p = 0.019$). The ANOVA revealed significant rule-based learning (significant main effect of Order: $F(1, 48) = 35.648$, $p < 0.001$, $\eta^2_p = 0.426$), participants showed faster RTs on high-probability pattern ($M = 314.56$ ms) compared with high-probability random trials ($M = 370.42$ ms). Participants were increasingly faster on high-probability pattern trials than on high-probability random trials as the task progressed (significant Order × Block interaction, $F(3, 144) = 15.089$, $p < 0.001$, $\eta^2_p = 0.239$). Rule-based learning was comparable between the GTS and HC groups (non-significant Order × Group interaction: $F(1, 48) = 0.465$, $p = 0.499$, $\eta^2_p = 0.010$; non-significant Order × Block × Group interaction: $F(3, 144) = 2.280$, $p = 0.116$, $\eta^2_p = 0.045$).

To check the potential influence of medication on learning, additional analyses were conducted. We excluded the GTS participants who took medication and their control counterparts. Then, on the medication-free sample ($n = 12$ in each group), we ran identical ANOVAs as on the whole sample separately for each learning score. The ANOVAs revealed identical results as those presented above, that is, increased statistical learning and comparable rule-based learning.

Furthermore, statistical learning scores were correlated with clinical measures in the GTS group. We focused on statistical learning as group differences emerged there between the GTS and HC groups. Clinical measures included the YGTSS score, the Rush total score, the DCI and disease duration. We found a positive correlation between statistical learning RT score and DCI ($r(23) = 0.430$, $p = 0.032$), while other correlations were not significant (all $ps > 0.105$).

3.2 | Neurophysiological results

Figure 3 presents the decoding performance and temporal generalisation results of statistical learning and rule-based learning separately in the two groups for the C-cluster data. The statistical learning classification was significantly above chance between 129 and 453 ms in the HC group and between 191 ms and 606 ms in the GTS group. The rule-based learning classification was significantly above chance

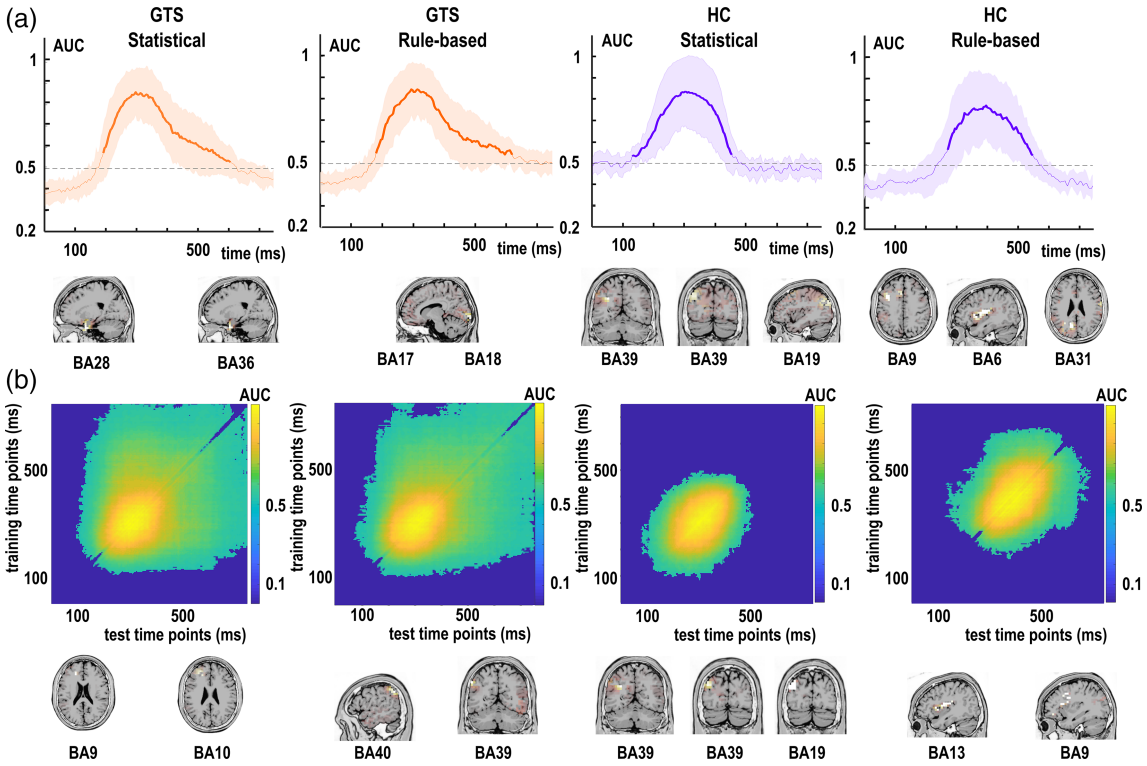

FIGURE 3 Neurophysiological results: decoding, temporal generalisation, and source localisation of statistical learning and rule-based learning for the C-cluster data. (a) Classification results of statistical information and rule-based information are presented separately for patients (Gilles de la Tourette syndrome, GTS in orange) and healthy control (HC, in purple) participants. Classification performance is quantified as AUC: higher AUC values represent better decoding. Time zero denotes the presentation of the target stimulus. Thicker lines indicate significant time windows ($p < 0.05$; two-sided cluster-based permutation). sLORETA source localisation for the time windows of significantly above-chance classification are illustrated below the horizontal axes. Sources are highlighted in white. (b) Temporal generalisation matrices of statistical information and rule-based information are depicted separately for GTS and HC participants. The plots show the degree to which the classifier when trained on a given time point (y-axis) generalises to time points in the trial (x-axis). The colours indicate the classifier performance. The diagonal (bottom left to top right) shows classification performance when the classifier is trained and tested on the same time points. Below the matrices, sLORETA source localisation results are presented based on time windows of high generalisation (see Neurophysiological results in the main text for details.)

from 273 ms to 551 ms in the HC group and 180 ms to 617 ms in the GTS group.

The temporal generalisation matrix of statistical learning in the HC group showed the highest accuracy (i.e., AUC >0.6) along the diagonal between ~200 and 400 ms after stimulus presentation. The above-chance classification gradually decreased to off-diagonal directions. The temporal generalisation matrix of rule-based learning in the HC group was comparable to statistical learning, albeit with a high accuracy cluster in ~300–500 ms. In the GTS group, the temporal generalisation matrix of statistical learning reached the highest accuracy (i.e., AUC >0.6) along the diagonal in the time window of ~200–400 ms. This above-chance classification then showed a ramping pattern that lasted until the end of the trial. The rule-based learning matrix of the GTS group showed a similar pattern to the statistical learning result: a central decoding cluster in ~200–400 ms that continued with a ramping activation until 750 ms after stimulus presentation.

To test the potential influence of medication on the neurophysiological results, we used the AUC values as a measure of decoding performance and contrasted them between the medicated ($n = 13$) and non-medicated ($n = 12$) GTS groups. We opted for this approach because excluding medicated participants from the RIDE-MVPA protocol would lead to an underpowered analysis. We could not detect a difference between the groups, neither in relation to statistical learning ($t(23) = 1.799$, $p = 0.090$) nor rule-based learning ($t(23) = 1.655$, $p = 0.117$).

Similarly to the behavioural analyses, C-cluster decodings related to statistical learning were correlated with the clinical measures, that is, the YGTSS score, the Rush total score, DCI and disease duration. We did not detect any significant correlations between clinical measures and C-cluster decodings (all *p*s >0.150).

MVPA performed on S-cluster and R-cluster data are described in the Supplementary Results and depicted in Figures S1 and S2.

4 | DISCUSSION

We investigated the simultaneous acquisition of sequential regularities in perceptual, motor and perceptual-motor coding levels of the neurophysiological signal in adults with GTS and controls. Two types

of regularities were presented in a visuomotor sequence learning task (Howard Jr. & Howard, 1997; Nemeth et al., 2013). Participants learnt those regularities and thus showed both successful 'statistical learning' and 'rule-based learning'. Importantly, statistical learning was larger in GTS than in HC, corroborating previous reports of hyper-learning (Shephard et al., 2019; Takács et al., 2018; Tóth-Fáber, Tárnok, Janacsek, et al., 2021). Interestingly, neurophysiological decoding showed that both enhanced statistical learning and unaltered rule-based learning might rely on atypical neural representations in GTS.

Representations were decoded at the perceptual (stimulus-related), motor (response-related) and stimulus–response translational levels. The latter can be interpreted (Vékony et al., 2023) as an abstract or not modality-specific representation that originates from encoding commonly coded features between stimuli and responses (Takacs et al., 2020). This level is thought to work in concert with modality-specific encodings to link perceptual and motor-based response coding systems (Conway, 2020; Frost et al., 2015; Vékony et al., 2023). The existence of an abstract code presents a computational advantage by allowing generalisation to overlapping events without modality-specific constraints (Eberhardt et al., 2017; Eggert et al., 2022; Takacs et al., 2020). Importantly, the temporal dynamics of the uncovered representations differed between GTS and HC participants at the abstract level (Figure 3). At the same time, decoding the modality-specific perceptual and motor codes revealed comparable neural representations between the two groups (Figures S1 and S2). This strengthens the notion (Beste & Münchau, 2018; Kleimaker et al., 2020) that stronger habitual behaviour in GTS is not an encapsulated motor problem but involves higher-order processes that do not rely on a modality-specific coding level.

Specifically, the decoded interval for statistical information was longer in the GTS group than in HC at the abstract level (Figure 3a). Similarly, rule-based information was decodable for a longer interval in GTS than in HC. Thus, representations of different sequential regularities were maintained longer in GTS than in HC, irrespective of whether the regularity was learnt in a superior (statistics) or a typical fashion (rule-based). Interestingly, the prolonged time windows in GTS indicated that statistical and rule-based representations were available even after response execution. The possible role of longer-maintained regularity representations in GTS is also relevant considering the temporal generalisation results (Figure 3b). In the HC group, the decoded representations were centred on the diagonal axes, with limited off-diagonal extensions. In GTS, the diagonally centred patterns showed ramping activities until the end of the trial. This adds to the decoding results (Figure 3a): representations of the statistical and rule-based regularities did not deactivate quickly upon response execution in GTS as it was seen among HC participants but showed a gradual decay. Memories are unstable and transient both after their formation (Robertson, 2018) and after their retrieval (Baena et al., 2021; Sara, 2000). In this state of instability, memories can be strengthened, weakened or integrated with overlapping memories (Baena et al., 2021). Prolonged activations of statistical and rule-based information in GTS could therefore signal a chance to modify S-R associations. Behavioural rewiring methods have already been explored in neurotypical populations (Szegedi-Hallgató et al., 2017).

The time scale of different brain activity patterns associated with sequential regularities reflects a combination of categorical and dimensional changes in the integration of the acquired knowledge (Maheu et al., 2019); namely, an early (< ∼150 ms) neurophysiological signal is a display of a relatively slow global integration (i.e., habituation). We observed a peak of decoding accuracy in this interval only when the perceptual coding level was used for classification (Figure S2). Later occurring time windows were suggested to reflect an increasingly local integration of the acquired knowledge (Maheu et al., 2019). During local integration, previously encoded associations can be gradually discounted to update the internal model of the environment. It has been shown that local integration time windows are sensitive to complex interrelations (e.g., transitional probabilities) (Kóbor et al., 2019, 2018; Maheu et al., 2019; Takács et al., 2021). The previously identified mid-latency (∼150–350 ms) and late (∼450–600 ms) windows related to sequential regularities (Kóbor et al., 2019, 2018; Maheu et al., 2019; Takács et al., 2021) were also observed in the current study, both among patients and control participants (Figure 3). However, in the GTS group, an even later window of 600–800 ms in each condition generalised to the interval of ∼200–800 ms in the respective pair of conditions. That is, adults with GTS did not only show atypically long activation of regularity representations but also a larger propensity to generalise the acquired information.

The extended generalisation in GTS could reflect either a longer integration of statistics and rules or additional processes (e.g., error monitoring or memory interference). Hyper-learning in GTS was observed as different error rates between high-probability random and low-probability random conditions. A decrease in accuracy for low-probability trials is thought to reflect the over-generalisation of the acquired high-probability transitions (Éltető et al., 2022; Horváth et al., 2020). However, extended generalisation occurred not only for statistics but also for rule-based information in GTS. Considering that rule-based learning was comparable between groups, it is unlikely that monitoring the increased error rate drove the lengthened availability and generalisation of regularity representations in GTS. Moreover, source localisation revealed that the decoded interval in GTS (Figure 3a) was not associated with areas of error monitoring (e.g., the anterior cingulate) but showed activity changes in the perirhinal (BA36) and entorhinal (BA28) cortices. For further discussion, please see the Supplementary Materials.

Taken together, structural differences in the perceived regularities were mapped differentially into spatiotemporal configurations of the neurophysiological activity. This approach is in line with spatiotemporal neuroscience that investigates neuro-mental relationship as spatiotemporal dynamics (Northoff et al., 2020a, 2020b). As both theoretical considerations (Conway, 2020) and the DPC model (Jiang & Rao, 2024) predicted, (low-level) statistical information was decoded with an earlier onset than (high-level) rule-based information in the HC group. In the GTS group, the two regularities were decoded in largely overlapping time windows. That is, there was no separation

between the more automatic, bottom-up statistical learning and the hierarchically superior rule-based learning. It is possible that concomitantly activating representations of statistics and rules lengthens the time necessary for integration (Tóth-Fáber, Tárnok, Janacsek, et al., 2021). Alterations of internal timescales and their deviation from their actual temporal characteristics in the external environment were observed in a number of psychiatric and neurological disorders, including depression and Parkinson's disease (Ibanez & Northoff, 2023; Scalabrini et al., 2023). In this context, signatures of atypical spatiotemporal dynamics at the whole-brain level were reported in GTS earlier: scale-free and aperiodic activity ('neural noise') during S-R integration was increased in patients (Adelhöfer et al., 2021; Münchau et al., 2021); and enhanced statistical learning was linked to a more optimally organised network architecture (Takacs et al., 2024). The consequences of blurred temporal boundaries between short and long scale predictions in GTS warrants further investigation that includes an even longer timescale for consolidation. Superior statistical learning in GTS was shown to modify resting-state architecture immediately after learning (i.e., scale of microconsolidation, Takacs et al., 2024). Additionally, children with GTS retained statistical information even after 1 year (Tóth-Fáber, Tárnok, Takács, et al., 2021). Therefore, mid- and long-term follow-up measures are needed to investigate how atypical learning in GTS might translate to day-to-day life (Takacs et al., 2021).

Long-term measures of memory consolidation could also highlight more direct connections between cognitive, clinical and neurophysiological levels. Here, we correlated statistical learning on the behavioural and neurophysiological levels with clinical measures, such as tic severity, DCI and disease duration. On the behavioural level, the DCI was positively correlated with statistical learning (in terms of RT), while tic severity did not show any correlation either with behavioural or neurophysiological measures. Interestingly, previous studies also did not find linear relationship between tics and spatiotemporal dynamics, such as network architecture and neural noise. It was proposed that these alterations at the neurophysiological level represent novel facets of GTS (Adelhöfer et al., 2021).

Taken together, we found hyperlearning of statistics in GTS patients and uncovered atypical representational dynamics at the not modality-specific coding level. The atypically activated representations were maintained longer, including a period when the stability of the memories decreased. We suggest that tracking the representations of hyperlearnt associations in GTS not only deepens our understanding of how habitual behaviour emerges but also presents a potential way to rewire maladaptive habits.

ACKNOWLEDGMENTS

This research was supported by the Deutsche Forschungsgemeinschaft (DFG) TA1616/2–1 (to Adam Takacs) and by FOR 2698 to Christian Beste and Alexander Münchau; the ANR grant awarded within the framework of the Inserm CPJ (N° ANR-22-CPJ1-0042-01); and the National Brain Research Programme by Hungarian Academy of Sciences (project NAP2022-I-1/2022) to Dezso Nemeth.

CONFLICT OF INTEREST STATEMENT

The authors declare no conflicts of interest.

DATA AVAILABILITY STATEMENT

The code for calculating the learning scores from the raw behavioural data, behavioural data, individual and group-level MVPA performance data, and codes for the analyses are available via the Open Science Framework: https://osf.io/fz2ta/?view_only=d697fd239ced4b7e8e5e40c3cd01e8b9. EEG data in various formats (raw, pre-processed, segmented, etc.) will be provided upon request.

ORCID

Adam Takacs https://orcid.org/0000-0002-6575-727X
Eszter Toth-Faber https://orcid.org/0000-0001-7538-9995
Dezso Nemeth https://orcid.org/0000-0002-9629-5856

REFERENCES

Adelhöfer, N., Paulus, T., Mückschel, M., Bäumer, T., Bluschke, A., Takacs, A., Tóth-Fáber, E., Tárnok, Z., Roessner, V., Weissbach, A., Münchau, A., Beste, C., & Weissbach, A. (2021). Increased scale-free and aperiodic neural activity during sensorimotor integration—A novel facet in Tourette syndrome. *Brain Communications*, *3*(4), fcab250.

Ariely, D. (2001). Seeing sets: Representation by statistical properties. *Psychological Science*, *12*(2), 157–162.

Baena, D., Cantero, J. L., & Atienza, M. (2021). Stability of neural encoding moderates the contribution of sleep and repeated testing to memory consolidation. *Neurobiology of Learning and Memory*, *185*, 107529.

Bartha, S., Bluschke, A., Rawish, T., Naumann, K. E., Wendiggensen, P., Bäumer, T., Roessner, V., Münchau, A., & Beste, C. (2023). Extra movements in healthy people: Challenging the definition and diagnostic practice of tic disorders. *Annals of Neurology*, *93*(3), 472–478.

Bayne, T., & McClelland, T. (2019). Ensemble representation and the contents of visual experience. *Philosophical Studies*, *176*, 733–753.

Beste, C., & Münchau, A. J. M. D. (2018). Tics and Tourette syndrome—surplus of actions rather than disorder? *Movement Disorders*, *33*(2), 238–242.

Bigdely-Shamlo, N., Mullen, T., Kothe, C., Su, K.-M., & Robbins, K. A. (2015). The PREP pipeline: Standardized preprocessing for large-scale EEG analysis. *Frontiers in Neuroinformatics*, *9*, 16.

Chang, T. Y., & Gauthier, I. (2022). Domain-general ability underlies complex object ensemble processing. *Journal of Experimental Psychology: General*, *151*(4), 966–972.

Christiansen, H., Hirsch, O., Philipsen, A., Oades, R. D., Matthies, S., Hebebrand, J., Ueckermann, J., Abdel-Hamid, M., Kraemer, M., Wiltfang, J., Graf, E., Colla, M., Sobanski, E., Alm, B., Rösler, M., Jacob, C., Jans, T., Huss, M., Schimmelmann, B. G., & Kis, B. (2013). German validation of the Conners adult ADHD rating scale–self-report: Confirmation of factor structure in a large sample of participants with ADHD. *Journal of Attention Disorders*, *17*(8), 690–698.

Conway, C. M. (2020). How does the brain learn environmental structure? Ten core principles for understanding the neurocognitive mechanisms of statistical learning. *Neuroscience and Biobehavioral Reviews*, *112*, 279–299.

Corbett, J. E., Utochkin, I., & Hochstein, S. (2023). *The pervasiveness of ensemble perception: Not just your average review*. Cambridge University Press.

Dehaene, S., Meyniel, F., Wacongne, C., Wang, L., & Pallier, C. J. N. (2015). The neural representation of sequences: From transition probabilities to algebraic patterns and linguistic trees. *Neuron*, *88*(1), 2–19.

Delorme, A., & Makeig, S. (2004). EEGLAB: An open source toolbox for analysis of single-trial EEG dynamics including independent component analysis. *Journal of Neuroscience Methods*, *134*(1), 9–21.

Delorme, C., Salvador, A., Valabregue, R., Roze, E., Palminteri, S., Vidailhet, M., de Wit, S., Robbins, T., Hartmann, A., & Worbe, Y. (2016). Enhanced habit formation in Gilles de la Tourette syndrome. *Brain*, *139*(2), 605–615.

Dippel, G., & Beste, C. (2015). A causal role of the right inferior frontal cortex in implementing strategies for multi-component behaviour. *Nature Communications*, *6*(1), 6587.

Eberhardt, K., Esser, S., & Haider, H. (2017). Abstract feature codes: The building blocks of the implicit learning system. *Journal of Experimental Psychology: Human Perception Performance*, *43*(7), 1275–1290.

Eggert, E., Takacs, A., Münchau, A., & Beste, C. (2022). On the role of memory representations in action control: Neurophysiological decoding reveals the reactivation of integrated stimulus–response feature representations. *Journal of Cognitive Neuroscience*, *34*(7), 1246–1258.

Éltető, N., Nemeth, D., Janacsek, K., & Dayan, P. (2022). Tracking human skill learning with a hierarchical Bayesian sequence model. *PLoS Computational Biology*, *18*(11), e1009866.

Farkas, B. C., Tóth-Fáber, E., Janacsek, K., & Nemeth, D. (2021). A process-oriented view of procedural memory can help better understand Tourette's syndrome. *Frontiers in Human Neuroscience*, *15*, 683885.

Foa, E. B., Huppert, J. D., Leiberg, S., Langner, R., Kichic, R., Hajcak, G., & Salkovskis, P. M. (2002). The obsessive-compulsive inventory: Development and validation of a short version. *Psychological Assessment*, *14*(4), 485–496.

Frost, R., Armstrong, B. C., Siegelman, N., & Christiansen, M. H. (2015). Domain generality versus modality specificity: The paradox of statistical learning. *Trends in Cognitive Sciences*, *19*(3), 117–125.

Goetz, C. G., Pappert, E. J., Louis, E. D., Raman, R., & Leurgans, S. (1999). Advantages of a modified scoring method for the rush video-based tic rating scale. *Movement Disorders: Official Journal of the Movement Disorder Society*, *14*(3), 502–506.

Goodman, W. K., Price, L. H., Rasmussen, S. A., Mazure, C., Fleischmann, R. L., Hill, C. L., Heninger, G. R., & Charney, D. S. (1989). The Yale-Brown obsessive compulsive scale: I. Development, use, and reliability. *Archives of General Psychiatry*, *46*(11), 1006–1011.

Hansmann-Roth, S., Kristjánsson, Á., Whitney, D., & Chetverikov, A. (2021). Dissociating implicit and explicit ensemble representations reveals the limits of visual perception and the richness of behavior. *Scientific Reports*, *11*(1), 3899.

Hartman, D. E. (2009). Wechsler adult intelligence scale IV (WAIS IV): Return of the gold standard. *Applied Neuropsychology*, *16*(1), 85–87.

Henin, S., Turk-Browne, N. B., Friedman, D., Liu, A., Dugan, P., Flinker, A., Doyle, W., Devinsky, O., & Melloni, L. (2021). Learning hierarchical sequence representations across human cortex and hippocampus. *Science Advances*, *7*(8), eabc4530.

Horváth, K., Kardos, Z., Takács, Á., Csépe, V., Nemeth, D., Janacsek, K., & Kóbor, A. (2020). Error processing during the online retrieval of probabilistic sequence knowledge. *Journal of Psychophysiology*, *35*(2), 1–15.

Howard, D. V., Howard, J. H., Jr., Japikse, K., DiYanni, C., Thompson, A., & Somberg, R. (2004). Implicit sequence learning: Effects of level of structure, adult age, and extended practice. *Psychology and Aging*, *19*(1), 79–92.

Howard, J. H., Jr., & Howard, D. V. (1997). Age differences in implicit learning of higher-order dependencies in serial patterns. *Psychology and Aging*, *12*(4), 634–656.

Ibanez, A., & Northoff, G. (2023). Intrinsic timescales and predictive allostatic interoception in brain health and disease. *Neuroscience and Biobehavioral Reviews*, *157*, 105510.

Jiang, L. P., & Rao, R. P. (2024). Dynamic predictive coding: A model of hierarchical sequence learning and prediction in the neocortex. *PLoS Computational Biology*, *20*(2), e1011801.

Kayser, J., & Tenke, C. E. (2015). On the benefits of using surface Laplacian (current source density) methodology in electrophysiology. *International Journal of Psychophysiology*, *97*(3), 171–173.

Khayat, N., Ahissar, M., & Hochstein, S. (2023). Perceptual history biases in serial ensemble representation. *Journal of Vision*, *23*(3), 7–7.

Khayat, N., Fusi, S., & Hochstein, S. (2021). Perceiving ensemble statistics of novel image sets. *Attention, Perception, & Psychophysics*, *83*, 1312–1328.

Kleimaker, M., Takacs, A., Conte, G., Onken, R., Verrel, J., Bäumer, T., Münchau, A., & Beste, C. (2020). Increased perception-action binding in Tourette syndrome. *Brain*, *143*, 1934–1945.

Kóbor, A., Horváth, K., Kardos, Z., Takács, Á., Janacsek, K., Csépe, V., & Nemeth, D. (2019). Tracking the implicit acquisition of nonadjacent transitional probabilities by ERPs. *Memory & Cognition*, *47*(8), 1546–1566.

Kóbor, A., Takács, Á., Kardos, Z., Janacsek, K., Horváth, K., Csépe, V., & Nemeth, D. (2018). ERPs differentiate the sensitivity to statistical probabilities and the learning of sequential structures during procedural learning. *Biological Psychology*, *135*, 180–193.

Leckman, J. F., Riddle, M. A., Hardin, M. T., Ort, S. I., Swartz, K. L., Stevenson, J., & Cohen, D. J. (1989). The Yale global tic severity scale: Initial testing of a clinician-rated scale of tic severity. *Journal of the American Academy of Child and Adolescent Psychiatry*, *28*(4), 566–573.

Maheu, M., Dehaene, S., & Meyniel, F. (2019). Brain signatures of a multiscale process of sequence learning in humans. *eLife*, *8*, e41541.

Maheu, M., Meyniel, F., & Dehaene, S. (2022). Rational arbitration between statistics and rules in human sequence processing. *Nature Human Behaviour*, *6*(8), 1087–1103.

Marco-Pallarés, J., Grau, C., & Ruffini, G. (2005). Combined ICA-LORETA analysis of mismatch negativity. *NeuroImage*, *25*(2), 471–477.

Mielke, E., Takacs, A., Kleimaker, M., Schappert, R., Conte, G., Onken, R., Künemund, T., Verrel, J., Bäumer, T., Beste, C., & Münchau, A. (2021). Tourette syndrome as a motor disorder revisited – Evidence from action coding. *NeuroImage. Clinical*, *30*, 102611.

Münchau, A., Colzato, L. S., AghajaniAfjedi, A., & Beste, C. (2021). A neural noise account of Gilles de la Tourette syndrome. *NeuroImage: Clinical*, *30*, 102654.

Nemeth, D., Janacsek, K., & Fiser, J. (2013). Age-dependent and coordinated shift in performance between implicit and explicit skill learning. *Frontiers in Computational Neuroscience*, *7*, 147.

Northoff, G., Wainio-Theberge, S., & Evers, K. (2020a). Is temporo-spatial dynamics the "common currency" of brain and mind? In quest of "spatiotemporal neuroscience". *Physics of Life Reviews*, *33*, 34–54.

Northoff, G., Wainio-Theberge, S., & Evers, K. (2020b). Spatiotemporal neuroscience–what is it and why we need it. *Physics of Life Reviews*, *33*, 78–87.

Opitz, A., Beste, C., & Stock, A.-K. (2020). Using temporal EEG signal decomposition to identify specific neurophysiological correlates of distractor-response bindings proposed by the theory of event coding. *NeuroImage*, *209*, 116524.

Ouyang, G., Herzmann, G., Zhou, C., & Sommer, W. (2011). Residue iteration decomposition (RIDE): A new method to separate ERP components on the basis of latency variability in single trials. *Psychophysiology*, *48*(12), 1631–1647.

Ouyang, G., & Zhou, C. (2020). Characterizing the brain's dynamical response from scalp-level neural electrical signals: A review of methodology development. *Cognitive Neurodynamics*, *14*(6), 731–742.

Park, J., Janacsek, K., Nemeth, D., & Jeon, H.-A. J. N. (2022). Reduced functional connectivity supports statistical learning of temporally distributed regularities. *NeuroImage*, *260*, 119459.

Parra, L. C., Spence, C. D., Gerson, A. D., & Sajda, P. (2005). Recipes for the linear analysis of EEG. *NeuroImage*, *28*(2), 326–341.

Pascual-Marqui, R. D., Esslen, M., Kochi, K., & Lehmann, D. J. M. (2002). Functional imaging with low-resolution brain electromagnetic tomography (LORETA): A review. *Methods and Findings in Experimental Clinical Pharmacology and Therapeutics*, *24*, 91–95.

Paulus, T., Bäumer, T., Verrel, J., Weissbach, A., Roessner, V., Beste, C., & Muenchau, A. (2021). Pandemic tic-like behaviors following social media consumption. *Movement Disorders*, *36*(12), 2932–2935.

Pedroni, A., Bahreini, A., & Langer, N. (2019). Automagic: Standardized preprocessing of big EEG data. *NeuroImage*, *200*, 460–473.

Perrin, F., Pernier, J., Bertrand, O., & Echallier, J. F. (1989). Spherical splines for scalp potential and current density mapping. *Electroencephalography and Clinical Neurophysiology*, *72*(2), 184–187.

Petruo, V., Takacs, A., Mückschel, M., Hommel, B., & Beste, C. (2021). Multi-level decoding of task sets in neurophysiological data during cognitive flexibility. *IScience*, *24*(12), 103502.

Pion-Tonachini, L., Kreutz-Delgado, K., & Makeig, S. (2019). The ICLabel dataset of electroencephalographic (EEG) independent component (IC) features. *Data in Brief*, *25*, 104101.

Prochnow, A., Bluschke, A., Weissbach, A., Münchau, A., Roessner, V., Mückschel, M., & Beste, C. (2021). Neural dynamics of stimulus-response representations during inhibitory control. *Journal of Neurophysiology*, *126*(2), 680–692.

Quentin, R., Fanuel, L., Kiss, M., Vernet, M., Vékony, T., Janacsek, K., Cohen, L. G., & Nemeth, D. (2021). Statistical learning occurs during practice while high-order rule learning during rest period. *NPJ Science of Learning*, *6*, 14.

Robertson, E. M. (2018). Memory instability as a gateway to generalization. *PLoS Biology*, *16*(3), e2004633.

Robertson, M., Banerjee, S., Kurlan, R., Cohen, D., Leckman, J., McMahon, W., Pauls, D. L., Sandor, P., & van de Wetering, B. (1999). The Tourette syndrome diagnostic confidence index: Development and clinical associations. *Neurology*, *53*(9), 2108.

Robertson, M. M., Eapen, V., Singer, H. S., Martino, D., Scharf, J. M., Paschou, P., Roessner, V., Woods, D. W., Hariz, M., Mathews, C. A., Črnčec, R., & Leckman, J. F. (2017). Gilles de la Tourette syndrome. *Nature Reviews Disease Primers*, *3*(1), 1–20.

Sara, S. J. (2000). Strengthening the shaky trace through retrieval. *Nature Review Neuroscience*, *1*(3), 212–213.

Scalabrini, A., De Amicis, M., Brugnera, A., Cavicchioli, M., Çatal, Y., Keskin, K., Pilar, J. G., Zhang, J., Osipova, B., Compare, A., Greco, A., Benedetti, F., Mucci, C., & Northoff, G. (2023). The self and our perception of its synchrony–beyond internal and external cognition. *Consciousness and Cognition*, *116*, 103600.

Sekihara, K., Sahani, M., & Nagarajan, S. S. (2005). Localization bias and spatial resolution of adaptive and non-adaptive spatial filters for MEG source reconstruction. *NeuroImage*, *25*(4), 1056–1067.

Shephard, E., Groom, M. J., & Jackson, G. M. (2019). Implicit sequence learning in young people with Tourette syndrome with and without co-occurring attention-deficit/hyperactivity disorder. *Journal of Neuropsychology*, *13*(3), 529–549.

Simor, P., Zavecz, Z., Horvath, K., Elteto, N., Török, C., Pesthy, O., Gombos, F., Janacsek, K., & Nemeth, D. (2019). Deconstructing procedural memory: Different learning trajectories and consolidation of sequence and statistical learning. *Frontiers in Psychology*, *9*, 2708.

Szegedi-Hallgató, E., Janacsek, K., Vékony, T., Tasi, L. A., Kerepes, L., Hompoth, E. A., Bálint, A., & Németh, D. (2017). Explicit instructions and consolidation promote rewiring of automatic behaviors in the human mind. *Scientific Reports*, *7*(1), 4365.

Takács, Á., Kóbor, A., Chezan, J., Éltető, N., Tárnok, Z., Nemeth, D., Ullman, M. T., & Janacsek, K. (2018). Is procedural memory enhanced in Tourette syndrome? Evidence from a sequence learning task. *Cortex*, *100*, 84–94.

Takács, Á., Kóbor, A., Kardos, Z., Janacsek, K., Horváth, K., Beste, C., & Nemeth, D. (2021). Neurophysiological and functional neuroanatomical coding of statistical and deterministic rule information during sequence learning. *Human Brain Mapping.*, *42*, 3182–3201.

Takacs, A., Mückschel, M., Roessner, V., & Beste, C. (2020). Decoding stimulus–response representations and their stability using EEG-based multivariate pattern analysis. *Cerebral Cortex Communications*, *1*(1), tgaa016.

Takacs, A., Münchau, A., Nemeth, D., Roessner, V., & Beste, C. (2021). Lower-level associations in Gilles de la Tourette syndrome: Convergence between hyperbinding of stimulus and response features and procedural hyperfunctioning theories. *European Journal of Neuroscience*, *54*, 5143–5160.

Takacs, A., Toth-Faber, E., Schubert, L., Tárnok, Z., Ghorbani, F., Trelenberg, M., Nemeth, D., Münchau, A., & Beste, C. (2024). Resting network architecture of theta oscillations reflects hyper-learning of sensorimotor information in Gilles de la Tourette syndrome. *Brain Communications*, *6*(2), fcae092.

Takács, Á., Yu, S., Mückschel, M., & Beste, C. (2022). Protocol to decode representations from EEG data with intermixed signals using temporal signal decomposition and multivariate pattern-analysis. *STAR Protocols*, *3*(2), 101399.

Tóth-Fáber, E., Tárnok, Z., Janacsek, K., Kóbor, A., Nagy, P., Farkas, B. C., Oláh, S., Merkl, D., Hegedűs, O., Nemeth, D., & Takács, A. (2021). Dissociation between two aspects of procedural learning in Tourette syndrome: Enhanced statistical and impaired sequence learning. *Child Neuropsychology*, *27*, 1–23.

Tóth-Fáber, E., Tárnok, Z., Takács, Á., Janacsek, K., & Németh, D. (2021). Access to procedural memories after one year: Evidence for robust memory consolidation in Tourette syndrome. *Frontiers in Human Neuroscience*, *15*, 715254.

Treder, M. S. (2020). MVPA-light: A classification and regression toolbox for multi-dimensional data. *Frontiers in Neuroscience*, *14*, 289.

Ullman, M. T., & Pullman, M. Y. (2015). A compensatory role for declarative memory in neurodevelopmental disorders. *Neuroscience and Biobehavioral Reviews*, *51*, 205–222.

Vékony, T., Takács, Á., Pedraza, F., Haesebaert, F., Tillmann, B., Mihalecz, I., Phelipon, R., Beste, C., & Nemeth, D. (2023). Modality-specific and modality-independent neural representations work in concert in predictive processes during sequence learning. *Cerebral Cortex*, *33*, 7783–7796.

Widmann, A., Schröger, E., & Maess, B. (2015). Digital filter design for electrophysiological data–a practical approach. *Journal of Neuroscience Methods*, *250*, 34–46.

Winkler, I., Brandl, S., Horn, F., Waldburger, E., Allefeld, C., & Tangermann, M. (2014). Robust artifactual independent component classification for BCI practitioners. *Journal of Neural Engineering*, *11*(3), 035013.

Winkler, I., Haufe, S., & Tangermann, M. (2011). Automatic classification of artifactual ICA-components for artifact removal in EEG signals. *Behavioral Brain Functions*, *7*, 1–15.

Wolff, N., Mückschel, M., & Beste, C. (2017). Neural mechanisms and functional neuroanatomical networks during memory and cue-based task switching as revealed by residue iteration decomposition (RIDE) based source localization. *Brain Structure Function*, *222*, 3819–3831.

SUPPORTING INFORMATION

Additional supporting information can be found online in the Supporting Information section at the end of this article.

How to cite this article: Takacs, A., Toth-Faber, E., Schubert, L., Tarnok, Z., Ghorbani, F., Trelenberg, M., Nemeth, D., Münchau, A., & Beste, C. (2024). Neural representations of statistical and rule-based predictions in Gilles de la Tourette syndrome. *Human Brain Mapping*, *45*(8), e26719. https://doi.org/10.1002/hbm.26719